Characterisation of transcriptional and chromatin events in relation to floral transition and identification of nuclear organisation determinants

del Prete, S.

Chapter 6

Molecular Determinants of the 3D Nuclear Organization in Arabidopsis

Javier Arpon[a], Kaori Sakai[a], Stefania Del Prete[a,b], Philippe Andrey[a], Valérie Gaudin[a]

Author affiliations

[a]Institut Jean-Pierre Bourgin, INRA, AgroParisTech, CNRS, Université Paris-Saclay, F-78000 Versailles, France

[b]Department of Plant Development and (Epi)Genetics, Swammerdam Institute for Life Sciences, University of Amsterdam, Amsterdam, the Netherlands

This chapter is part of a paper in preparation.

Abstract

The interphase cell nucleus is a dynamic organelle in terms of size, shape, composition and spatial organisation. Despite impacts on gene regulation, the mechanisms and the molecular determinants controlling the tridimensional nuclear organisation are still elusive. Here we searched for determinants involved in the heterochromatin distribution in the plant model *Arabidopsis thaliana*. We used confocal microscopy coupled with innovative 3D spatial statistical tools and a reverse genetic approach with three candidates proteins, *CRWN1*, *CRWN2* and *KAKU1*, located at the periphery of the cell nucleus and involved in nuclear shape. The *crwn1* and *crwn2* mutations affect constitutive heterochromatin features and impact the spatial positioning of chromocenters relative to each other, whereas *kaku1* mutations predominantly impact nuclear shape in mesophyll cells, but not the spatial distribution of chromocenters

Introduction

In eukaryotes, the cell nucleus is a specialized and well-organized organelle (i) ensuring the critical genome keeper function; (ii) hosting the functions involved in cellular responses and (iii) involved in a dynamic transmission of the genome throughout the cell cycle. Beyond the historical partitioning of the genome into euchromatic and heterochromatic compartments (Heitz, 1929) and chromosome territories (Boveri, 1909; Cremer and Cremer, 2010), the development of 3C-derivative technologies has revealed that the nuclear genome is compartmentalized into topological chromatin units, which are based on spatial proximity or interactions with non-DNA nuclear structures (Dixon et al., 2016; Gonzalez-Sandoval and Gasser, 2016; Sati and Cavalli, 2016). For instance, topologically associated domains (TADs), lamina-associated domains (LADs) (Pickersgill et al., 2006; Guelen et al., 2008), nucleolus-associated chromatin domains NADs (Nemeth et al., 2010; van Koningsbruggen et al., 2010; Pontvianne et al., 2016), and more recently, pericentromere-associated domains (PADs) (Wijchers et al., 2015) have been reported. Most of them are largely invariant and conserved among the different cell types (i.e. TADs) (Dixon et al., 2016), while some have a tendency to be constitutive (i.e. LADs, PADs) (Meuleman et al., 2013), for others cell-type specificities have been reported (i.e. LADs, PADs) (Wijchers et al., 2015). These recent data question (i) the relationship between the genome scaffolding and its biological functions, (ii) the organization of the genome in the 3-dimensional (3D) space of the interphase cell nucleus, and (iii) the molecular actors involved in this process. Furthermore, the interphase cell nucleus is a dynamic and plastic organelle, in terms of shape, size, composition, and even, positioning in the cellular volume (Tamura et al., 2013; Del Prete et al., 2014), thus questions about the mechanism behind the dynamics of its organization are arising.

The rules governing the genome organization in the 3D nuclear space have been investigated but remain elusive. Radial and conserved positioning of chromosomes were described in human and primate nuclei (Tanabe et al., 2002; Cremer and Cremer, 2010). In plants a frequent pairwise association of chromosome arms has been documented in *A. thaliana* triploid endosperm nuclei (Baroux et al., 2016), whereas a random arrangement of chromosome territories

(CTs) was observed in Arabidopsis somatic cell nuclei (Pecinka et al., 2004; Schubert et al., 2012). At a smaller scale, the spatial patterning of chromocenters (CCs), which is a constitutive heterochromatic compartments visible by DAPI staining and mainly enriched in centromeric DNA repeats and pericentromeric regions, was described as more regular than under a completely random model, suggesting an underlying organization (Andrey et al., 2010). Recently, it was shown that during mouse cell differentiation, regions associated with the pericentromeric satellites increasingly overlap with LADs, suggesting a displacement towards the repressive nuclear peripheral compartment (Wijchers et al., 2015). This observation is in agreement with a bunch of data suggesting that the nuclear periphery has a repressive role. The 3D nuclear landscape indeed impacts the transcriptional gene activity. For instance, the oscillation of the transcriptional status of clock-regulated genes seems to correlate with their movement towards the nuclear periphery (Aguilar-Arnal et al., 2013; Zhao et al., 2015). During vernalization, the cold exposure required by some plant species in order to flower, the transcriptional repression of the flowering repressor FLOWERING LOCUS C (FLC) by Polycomb proteins is associated with a clustering of the FLC loci in the nuclear space (Rosa et al., 2013).

The nucleus is delineated by the nuclear envelope (NE) and by a filamentous protein network located to the inner surface of the NE, the lamina. On the outer surface of the NE, the cytoskeleton interacts with NE-associated proteins, some of which are connected with the lamina, thus forming an intricate protein network between the outside and the inside of the nucleus (Ciska and Moreno Diaz de la Espina, 2014). The nuclear periphery (NP) plays important roles in the mechanical properties of the nucleus and in cell migration. It mediates responses to cellular stress and is also involved in the exchange with the outside of the nucleus. Furthermore, NP-associated proteins participate to the control of nuclear size and morphology both in animals and plants. In *Arabidopsis thaliana*, mutations in components of the linker of nucleoskeleton and cytoskeleton (LINC) complex (Gruenbaum and Medalia, 2015; Tamura et al., 2015; Zhou et al., 2015) or in the Nuclear Matrix Constituent Protein1 (NMCP1) (Ciska and Moreno, 2013) family affect nuclear morphology. The four A. *thaliana* CROWDED NUCLEI proteins (originally named LITTLE NUCLEI, LINC) are coiled-coil proteins belonging to NMCP family. The CRWN proteins play

crucial role in nuclear morphology and organization although having a different localization (Masuda et al., 1997; Dittmer et al., 2007; Ciska and Moreno, 2013; Wang et al., 2013). CRWN1/LINC1 and CRWN4 are mainly located at the nuclear periphery, and some interaction between CRWN1 and components of the LINC complex were reported at the nuclear envelope, but small CRWN1 and CRWN4 nucleoplasmic fractions were also reported, according to cell types (Sakamoto and Takagi, 2013; Graumann, 2014; Zhao et al., 2016). CRWN2 and CRWN3 are mainly localized in the nucleoplasm (Sakamoto and Takagi, 2013). Plant nuclear envelope-associated proteins (NEAP), interacting with LINC components, have been recently identified, which also participate to nuclear morphology (Pawar et al., 2016). Finally, KAKU1 is a plant-specific class-XI myosin phylogenetically distant from the other members of this family, located at the nuclear periphery, which also controls nuclear shape and organization (Tamura et al., 2013; Haraguchi et al., 2016). To which extend the genome organization is impacted in mutants with altered nuclear size and morphology remains to be established to further decipher the interplay between the 3D space and the plant genome organization.

Here, we thus investigated the relationship between the cell nuclear morphology and the genome organization by focusing on the Arabidopsis constitutive heterochromatin compartment, which is a structural, dynamic and functional compartment (Del Prete et al., 2014). Indeed, the Arabidopsis chromocenters serve as anchorage sites for chromatin loops in a rosette model (Fransz et al., 2002) and studies have reported that these structures vary in size, shape, number or compaction depending on cell differentiation and various developmental and environmental cues (Del Prete et al., 2014). Since the components of the nuclear periphery largely impact nuclear morphology, we extensively characterized the 3D nuclear organizations of the CCs in *crwn1, crwn2, crwn1 crwn2* and *kaku1* mutants using 3D image analyses, spatial statistics and modelling approaches. Morphological parameters of the cell nucleus obtained in 3D in the different genetic backgrounds were compared to wild-type nuclei and discussed relatively to previous 2D studies. The CC distributions were characterized by using four spatial descriptors in the different mutant backgrounds and allowed to identify some critical molecular determinants. We show that the loss-of-function of CRWN proteins family

determines a large-scale remodelling of the 3D nuclear landscape wherease for *kaku1* mutant the main change was detected on nuclear shape.

Results

The *crwn1* and *crwn2* mutations have globally similar and additive effects on 3D nuclear size and shape

The nuclear morphology is sensitive to various cellular parameters such as cell type, cell differentiation and developmental stage of plants. To minimize possible developmental effects on the nuclear morphology and get a population of nuclei as homogeneous as possible, we analysed mesophyll cell nuclei from rosette leaves of plants after bolting. This choice allowed us to get observations independently of the differences in flowering time between wild-type and mutant plants. We performed cryosections to identify cell types and performed confocal microscopy image acquisition on a quite homogeneous cell nuclei population. From the quantification of the nuclear size in 3D we observed that the nuclear volume of *crwn1* and *crwn2* was similar, but significantly reduced compared to the wild-type plants (Figure 1A). Furthermore, the nuclear volume in the double mutant *crwn1 crwn2* was significantly smaller compared with each of the single mutants (Figure 1A). Interestingly, a reduced variability in the nuclear size was observed in the single and double mutants compared to the control line. Overall, our 3D size analysis was in agreement with a previous report based on 2D area measurements (Dittmer et al., 2007). However, different studies also reported absence of size alteration in *crwn2* nuclei (Sakamoto and Takagi, 2013; Wang et al., 2013). The discrepancy between our results with these last two studies may be due to the use of 3D versus 2D approaches, but also on the different biological material used.

To evaluate the impact of the *crwn1* and *crwn2* mutations on nuclear shape, we measured the nuclear sphericity defined as a normalized measure of the similarity between an arbitrary 3D shape and a perfect sphere. All mutants presented an increased nuclear sphericity, but at varying degrees (Figure 1B). The smallest increase was observed in *crwn2* while the largest in *crwn1 crwn2*,

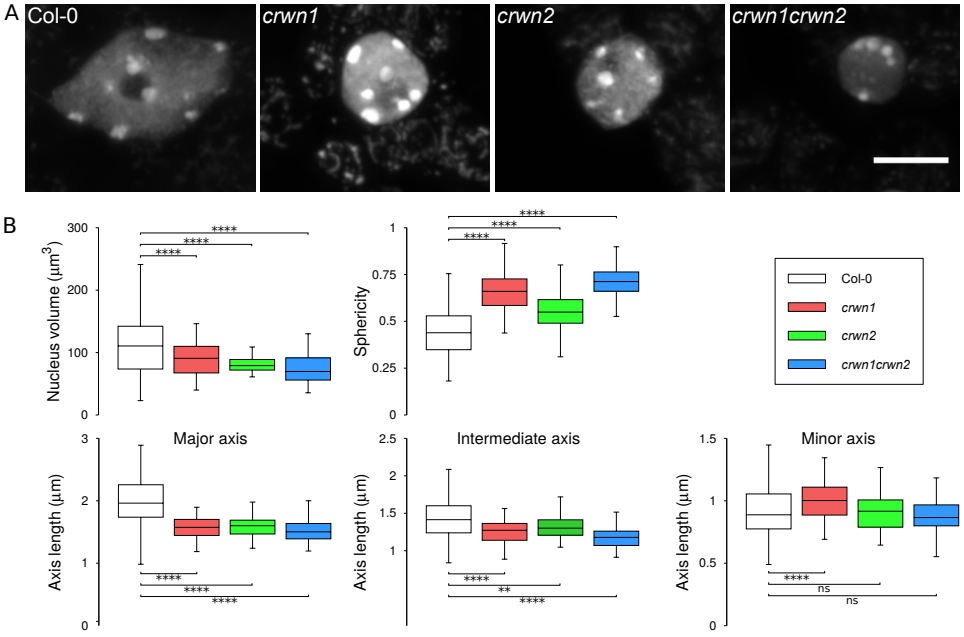

Figure 1: Morphology of mesophyll cell nuclei in *crwn1* and *crwn2* single and double mutants.

A) DAPI-stained nuclei in wild-type plants and *crwn1*, *crwn2*, and *crwn1 crwn2* mutants. The images show maximum intensity projections of 3D confocal image stacks. Scale bar, 5 µm.

B) Distributions of nuclear size and shape parameters in the four genotypes. Wilcoxon test used to analyse the differences between wild-type and mutants lines. **ns,** $p > 0.05$; *, $p < 0.05$; **, $p < 0.01$; ***, $p < 0.001$.

suggesting additive effects on nuclear shape of the *crwn1* and *crwn2* mutations, as observed for nuclear size. The 3D shapes of these mutants were in agreement with previous reports, which measured the 2D circularity (Dittmer et al., 2007; Wang et al., 2013).

We then examined whether the observed changes in nuclear shape and size were accompanied by other morphological alterations. We computed for each nucleus the length of the three main axes of the equivalent inertia ellipsoid. The three mutants exhibited a marked reduction in the length of the major (i.e., longest) and intermediate (second longest) axes, with an increased homogeneity in the distribution of these two parameters (Figure 1B). There was no difference between the two single mutants but the lengths of the major and intermediate axes were smaller in the double compared to the single mutants, thus strongly

supporting the hypothesis that the two single mutations had additive effects on nuclear size. Only *crwn1* nuclei presented a significantly altered minor axis length, which was larger compared to the wild-type nuclei. Overall, the global reduction of the first two axis lengths and the unchanged or increased length of the minor axis suggested that the observed increased sphericity was at least partially due to changes in the global shape of *crwn* nuclei.

The *crwn1* and *crwn2* mutations affect constitutive heterochromatin features

To quantify the impact of the *crwn* mutations on constitutive heterochromatin, we measured the number of chromocenters (CCs). There was no significant alteration of the CCs number per nucleus in the *crwn1* mutant compared to wild type plants but this number decreased in the *crwn2* mutant and dropped even more in the *crwn1 crwn2* mutant (Figure 2A). However, the density (average number of chromocenters per nuclear volume unit) was actually increased in the three mutants (Figure 2B). This result suggested that, proportionally to nuclear volume, there was more chromocenters in the mutants than in the wild-type plants, a counter-intuitive result given the reduction in the raw number of chromocenters (Figure 2A; (Wang et al., 2013)). In addition, we found that the CC density increased to a comparable level in the three mutants (two-sided Wilcoxon test: *crwn1* vs. *crwn2*: P=0.38; *crwn1* vs. *crwn1 crwn2*: P=0.16; *crwn2* vs. *crwn1 crwn2*: P=0.73). Thus, these mutants shared a common proportionality law between nuclear volume and the absolute number of chromocenters.

We next quantified the nuclear space occupied by the constitutive heterochromatin fraction. The two single mutants exhibited pronounced opposite differences compared to the wild-type plants in the volume of individual chromocenters, with an increase in *crwn1* and a decrease in *crwn2* (Figure 2C). Normalizing chromocenter volume by nuclear volume abolished the difference observed between wild-type and *crwn2* plants, suggesting that chromocenter size was strongly correlated to nuclear size in *crwn2* (Figure 2D). In the double mutant, the reduction of the absolute chromocenter volume was less pronounced than in *crwn2*, and the increase of relative size was similar to that in *crwn1*, possibly suggesting an additive effect of the two single mutations on

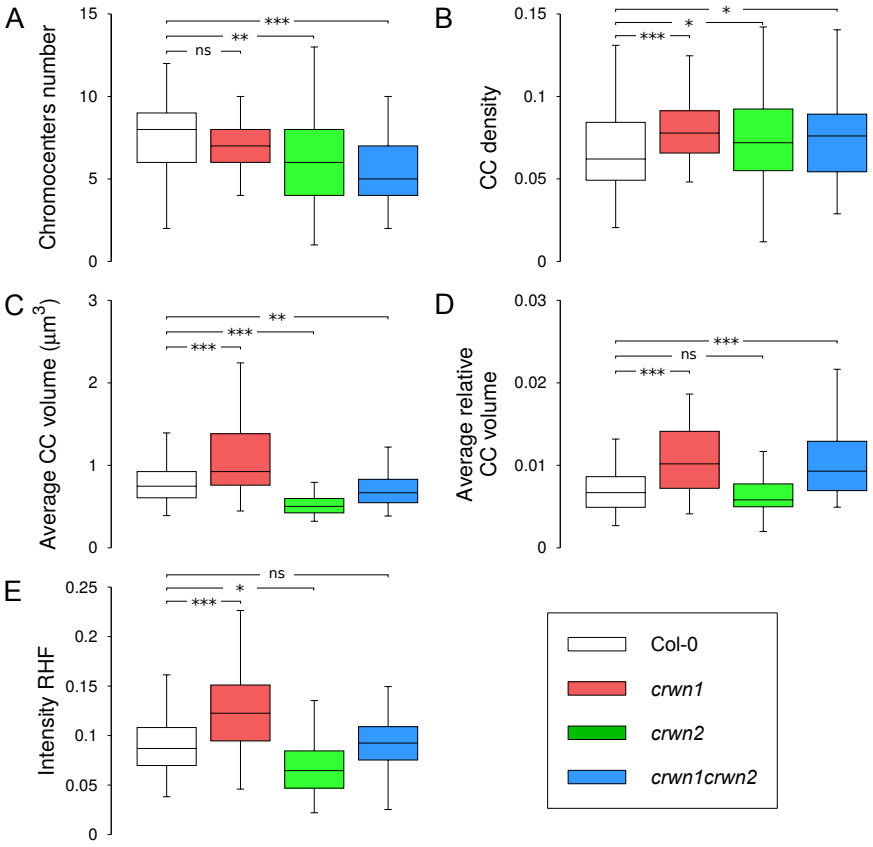

Figure 2: Heterochromatin features of mesophyll cell nuclei in *crwn1* and *crwn2* single and double mutants.
A) Number of chromocenters.
B) Density of chromocenters (number per unit volume).
C) Average volume of chromocenters.
D) Average normalized volume of chromocenters.
E) Intensity relative heterochromatin fraction.

chromocenter size. We then examined the proportion of total nucleus intensity in chromocenters, intensity heterochromatin fraction (IRHF). The IRHF was significantly higher in *crwn1* compared to wild-type (Figure 2E), in agreement with having similar numbers of chromocenters, but larger, and in smaller nuclei.

By contrast, the IRHF was smaller in *crwn2* compared to the wild-type, again a consistent result with having a smaller number of chromocenters with an unaltered relative individual volume. Both effects were cancelled in the double

mutant, for which there was no IRHF difference to wild-type plants. The same results were observed when computing the relative heterochromatin fraction by weighting voxels by their intensities. Overall, these results point to strong effect of the single mutations on different heterochromatin features, leading to opposite variations in the relative amounts of heterochromatin.

crwn1 and *crwn2* impact the relative positioning of chromocenters in the nuclear space

Given the large and diverse changes that we observed in the *crwn* mutants, we questioned whether the spatial organization of heterochromatin was also affected. We compared the spatial patterns of chromocenters observed in each genotype to expectations under a completely random distribution model. This was achieved by virtually randomizing, for each nucleus, the chromocenter positions within its corresponding nuclear shape. Comparisons between observed and randomized patterns were performed using spatial descriptors based on distance measurements. The variations between nuclei morphology and heterochromatin features were taken into account by computing a Spatial Distribution Index (SDI) for each nucleus and each descriptor. The SDI is a normalized measure that quantifies the agreement between an observed chromocenter pattern and the random model (Andrey et al., 2010).

We first compared observed chromocenter patterns to a completely random model of chromocenter distribution by measuring empty spaces between chromocenters. To this end, we measured the *F*-function, the cumulative distribution function of the distance between arbitrary nuclear position and the nearest chromocenter. In wild-type nuclei, the distribution of the *F*-based SDI was concentrated towards 0 (Figure 3A), meaning that empty spaces between chromocenters tended to be smaller than expected under a completely random distribution. This showed that chromocenters in mesophyll cells had a more regular spatial distribution as compared with complete randomness, in agreement with our previous results on isolated leaf cell nuclei (Andrey et al., 2010). While the same trend was observed in the *crwn1* mutant, there was no difference in the observed *F*-SDI distribution and the distribution expected under a completely random organization in *crwn2*, revealing an unaltered spatial distribution of

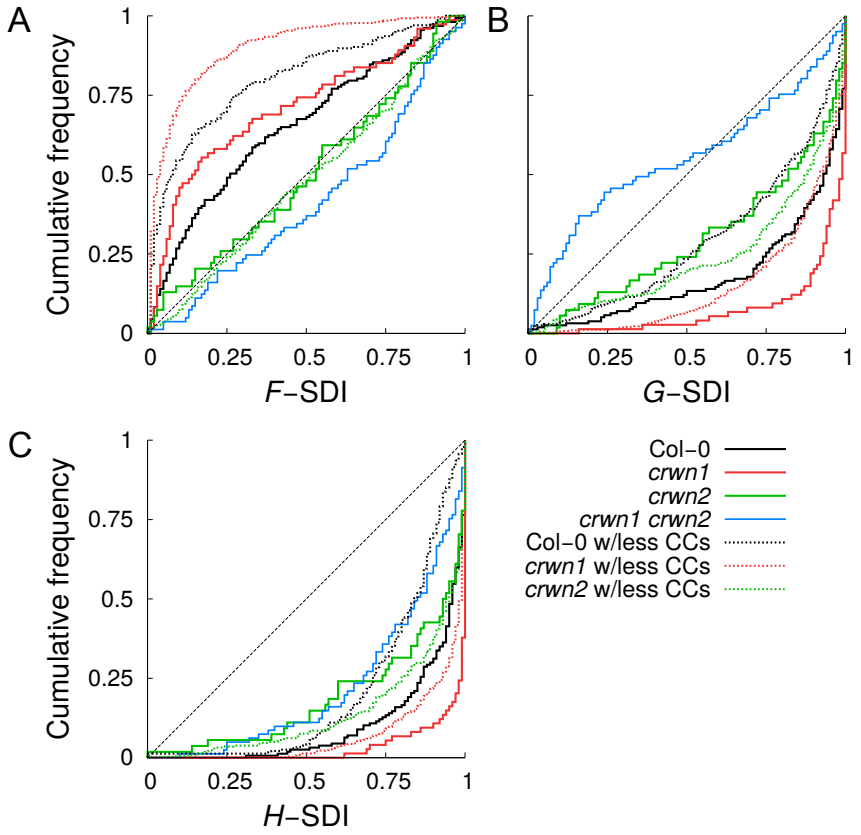

Figure 3: Effects of *crwn1* and *crwn2* mutations on the 3D spatial organization of chromocenters: statistical comparison of observed patterns with a completely random organization.

The graphs show the cumulative distribution of the Spatial Distribution Index (SDI) computed from the cumulative distribution function of (A) the radius of the empty spaces between chromocenters; (B) the distance to the nearest chromocenter; (C) the interdistances between all chromocenters. The dashed diagonal line corresponds to the expected SDI distribution under a completely random organization of the chromocenters.

chromocenters compared to wild-type nuclei. In the *crwn1 crwn2* mutant, the distribution of the *F*-SDI was slightly shifted towards 1, suggesting a reversed trend in this spatial organization with a tendency towards chromocenters clustering.

Next, we used the *G*-function, which is the cumulative distribution function of the distance between each chromocenter and its closest neighbour, to further

validate these results. The *G*-based SDI distribution (Figure 3B) confirmed a more regular organization of chromocenters compared to complete randomness in both wild-type and *crwn1* nuclei. As opposed to *F*-SDI results, the *G*-SDI analysis revealed that there was a significant difference between the chromocenter distribution in *crwn2* and complete randomness. Chromocenters in this mutant exhibited a trend towards regularity as in Col-0 and *crwn1* genotypes. In the *crwn1 crwn2* mutant, the *G*-SDI distribution showed smaller distances to the nearest chromocenter compared to complete randomness, confirming the tendency towards clustering of chromocenters, contrary to the wild-type plants.

Both the *F*- and the *G*- functions are descriptors that provide a local scale quantification of spatial organizations. To determine whether there were also alterations at global scale in the spatial distribution of chromocenters, we compared observed patterns to model expectations using the *H*-function, the cumulative distribution function of all inter-distances between chromocenters (Figure 3C). In the wild-type plants as in all three mutants, the *H*-based SDI was condensed towards 1, corresponding to larger inter-distances between chromocenters compared to complete randomness. As opposed to the results obtained with the local descriptors, nuclei in the double mutant showed the same trend than wild-type nuclei, suggesting that alterations in the spatial distribution of chromocenters in the *crwn1 crwn2* mutant were at a local scale and did not affect the large-scale organization.

Since the SDI is structurally equivalent to a *p*-value, it may potentially be affected by variations in the number of objects in the analysed patterns. Therefore, we examined to what extent differences in SDI distributions between wild-type and mutant nuclei could result from observed differences in the numbers of chromocenters, since *crwn1 crwn2* had a much reduced number of chromocenters (Figure 2A). We re-ran the spatial analyses after removing two randomly selected chromocenters in Col-0 and *crwn1* nuclei and one chromocenter in *crwn2* nuclei. The number of chromocenters removed corresponded to the observed average differences between the selected line and the double mutant (Figure 2A). The obtained SDI distributions were affected to various extents but their relative positions compared with the random model were not altered (Figure 3 and Figure 4D, *dotted lines*). The distributions in the

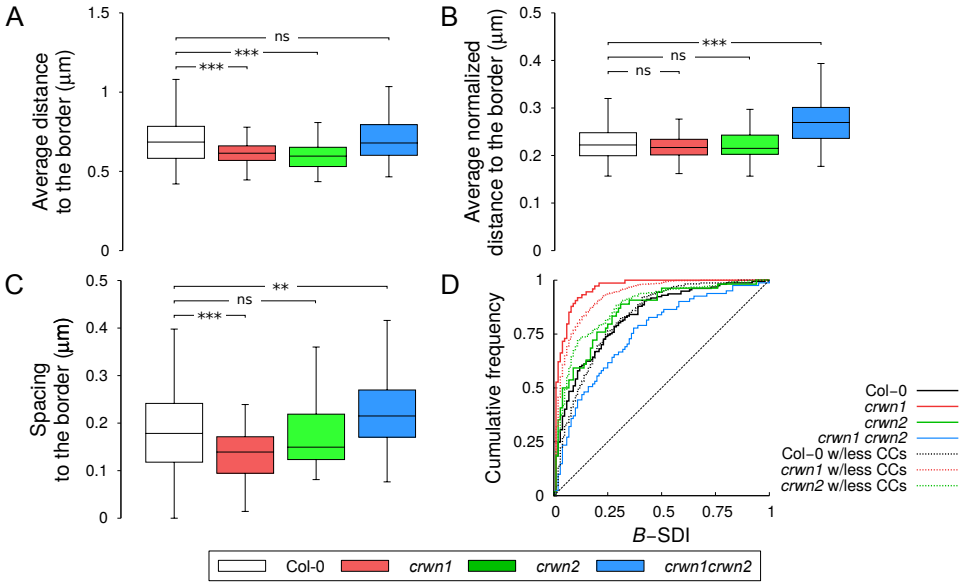

Figure 4: Spatial interactions between chromocenters and nuclear periphery in wild-type Col-0 and *crwn* mutants.
A) Average distance between chromocenter centroid and nuclear boundary.
B) Same as (A) following normalization by nucleus equivalent radius.
C) Average spacing between chromocenter and nuclear boundaries.
D) Statistical comparison of observed patterns with a completely random organization: cumulative distributions of the SDI computed from the cumulative distribution function of the distance between chromocenter centroid and nuclear boundary.

wild-type plants and in the single mutants were still markedly distinct from the distribution observed in the *crwn1 crwn2* mutant. We concluded that the observed SDI distributions in *crwn1 crwn2* nuclei were unlikely to result from differences in the number of chromocenters.

crwn1 and *crwn2* impact the distance between the chromocenters and the nuclear periphery

Due to the localisation of CRWN1 at the nuclear periphery, we examined whether the changes observed at the local scale in the distribution of chromocenters could be linked with alterations in their positioning relatively to the nuclear periphery. We thus examined the positions of chromocenters relatively to the nuclear border. We observed that the average distance from each chromocenter to nuclear border was significantly reduced at a comparable level

in the two single mutants but remained unaltered in the double mutant (Figure 4A). However, normalizing this distance by the equivalent radius of the nucleus abolished the differences in the single mutants (Figure 4B). The spacing between chromocenters and nuclear periphery, as measured by the surface distance, was reduced in *crwn1*, unaltered in *crwn2*, and increased in *crwn1 crwn2* (Figure 4C). This was consistent with the observed differences in size and in average distance to the border. Overall, these results suggested that the CRWN1 and CRWN2 proteins have similar effects in mediating a global scaling between nuclear volume and the distance between chromocenter's barycenter and nuclear periphery.

Since proximity to the periphery can occur by pure chance with a high probability in a 3D domain, we examined the statistical significance of the peripheral positioning of chromocenters. We used the *B*-function, the cumulative distribution function of the distance between the chromocenter's barycenter and the nearest point at the boundary of the nucleus, and computed the *B*-SDI against the completely random model. The obtained results showed that the *crwn1* mutation induced a significantly more peripheral localization of chromocenters as compared with the wild-type. On the contrary, there was no change in the peripheral localisation of chromocenters in *crwn2* and chromocenters were significantly more internal in the double mutant (Figure 4D). Similarly to what was observed with the *F*-, *G*-, and *H*-functions, the observed shifts in the *B*-based SDI distributions could not result from observed differences in the numbers of chromocenters (Figure 4D, *dotted lines*).

kaku1 mutations predominantly impact nuclear shape in mesophyll cells

KAKU1 encodes a plant-specific myosin (Myosin XI-i) localised at the nuclear periphery, with a role of linker between the nuclear membrane and the cytoskeleton. It was shown that the SUN-WIP-WIT2-Myosin XI-i complex influences the nuclear shape (Tamura et al., 2013). To further decipher the determinants of 3D nuclear morphology and spatial organization of constitutive heterochromatin, we analysed the *kaku1-3* and *kaku1-4* mutants. The nuclear size was significantly increased in the *kaku1-3* mutant, whereas no difference was

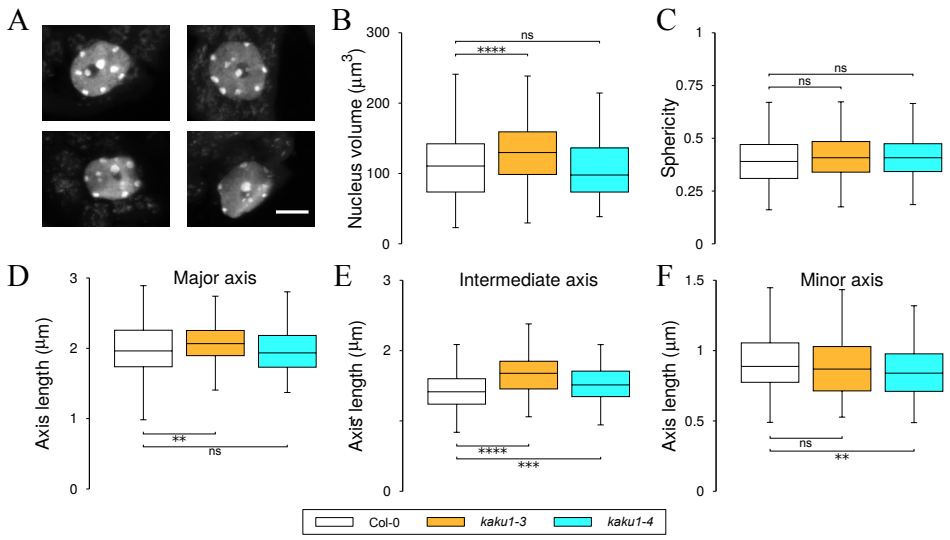

Figure 5: Nuclear morphology in the *kaku1-3* and *kaku1-4* mutants.
A) DAPI-stained nuclei of mesophyll cells in *kaku* mutants. The images show maximum intensity projections of 3D confocal image stacks. Scale bar, 5 µm.
B) Size and shape nuclear measurements. Statistical tests used to analyse the differences between wild-type and mutants lines. *, $p < 0.05$; **, $p < 0.01$; ***, $p < 0.001$; ****, < 0.0001.

observed in the *kaku1-4* mutant (Figure 5B). None of the two mutations altered the 3D sphericity of the nuclei (Figure 5A). This observation was surprising since an increased 2D circularity has been previously reported in *kaku1-1* nuclei (Tamura et al., 2013). However, local surface irregularities and invaginations had also been reported in this mutant (Tamura et al., 2013).

Our sphericity parameter takes in consideration the shape surface and in case of less regular surface the value decreases towards zero. Therefore, we also quantified global shape parameters. The elongation (length ratio between the largest and the intermediate axes) was significantly decreased in *kaku1-3* and *kaku1-4* nuclei as compared to wild-type nuclei, in accordance with the previously reported nearly spherical shape of these mutants (Tamura et al., 2013). Analysing separately the lengths of the three principal axes revealed that the elongation reduction resulted essentially from an increased intermediate axis length (Figure 5E). Overall, our results suggested that KAKU1 contributes mainly to determine the nuclear shape.

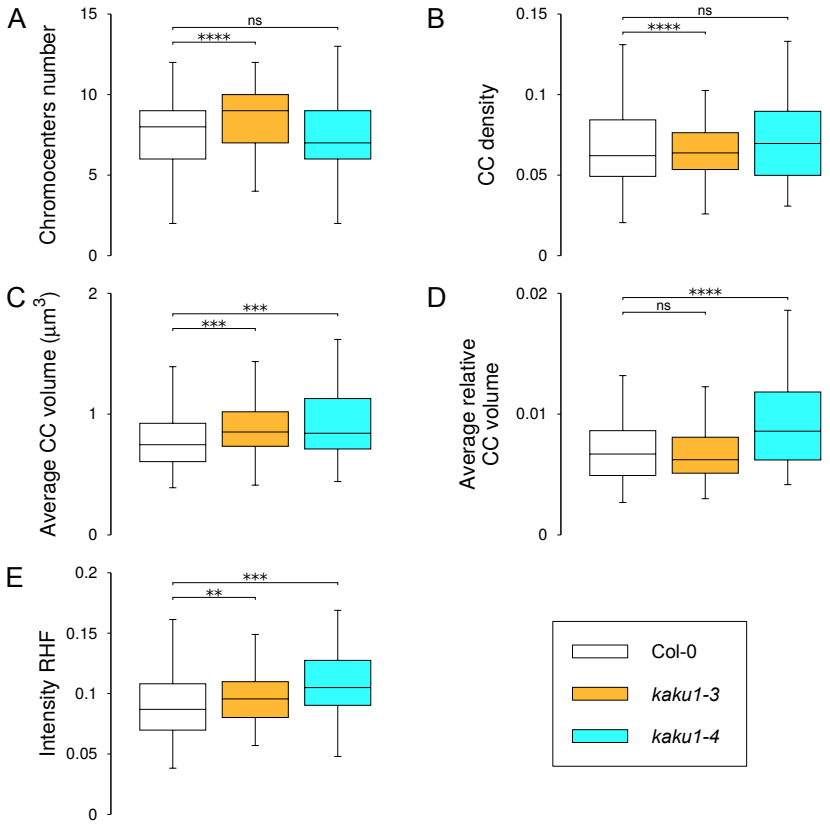

Figure 6: Effects of *kaku1-3* and *kaku1-4* mutations on heterochromatin features in mesophyll cell nuclei.
A) Number of chromocenters.
B) Density of chromocenters (number per unit volume).
C) Average volume of chromocenters.
D) Average normalized volume of chromocenters.
E) Intensity relative heterochromatin fraction.

Constitutive heterochromatin is affected in *kaku1* mutants

Given the shared effects on nuclear morphology of the *crwn* and *kaku1* mutations and the influence of CRWN1 on heterochromatin features, we next examined whether the *kaku1* mutants presented altered constitutive heterochromatin features.

There was no difference, either in the absolute or in the relative number (density) of chromocenters in the *kaku1-4* mutant (Figure 6A-B). By contrast, the number

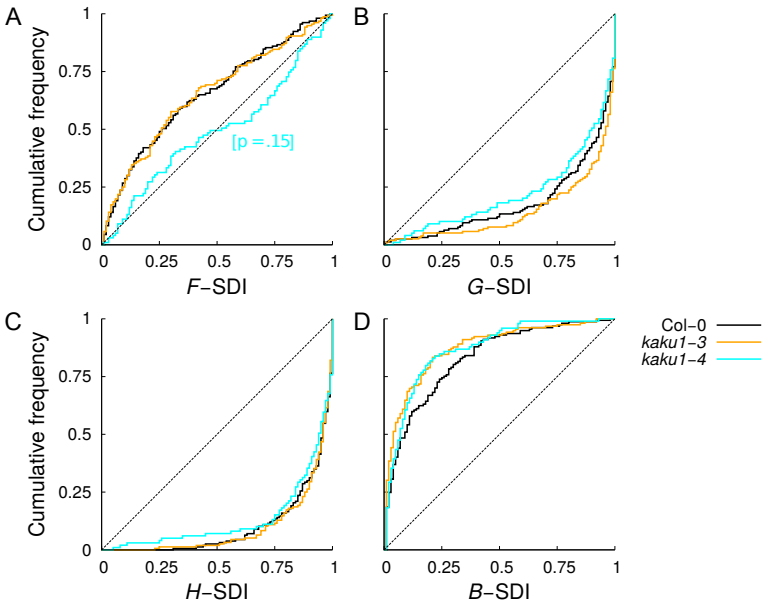

Figure 7: The global spatial distribution of chromocenters was not altered in the kaku mutants.

The graphs plot the cumulative distribution of the Spatial Distribution Index (SDI) obtained by comparing observed chromocenter patterns to completely random patterns. The SDI is computed from the cumulative distribution function of (A) the radius of empty spaces; (B) the distance to the nearest chromocenter; (C) the distance to any other chromocenter; (D) the distance to the border of the nucleus. The dashed diagonal line corresponds to the expected SDI distribution under a completely random organization of the chromocenters.

of chromocenters was increased in *kaku1-3* (Figure 6A). This was likely a scaling effect of the increased nuclear size, since the CC density was not different compared to wild-type plants (Figure 6B).

Chromocenters were bigger in the *kaku1-3* mutant (Figure 6C), but this was again probably a scaling effect as normalizing chromocenter size by nuclear volume abolished the difference (Figure 6D).

In *kaku1-4*, chromocenter size was increased to the same level as in *kaku1-3* (Figure 6C). Given the unaffected nucleus size, this resulted in an increased relative volume of chromocenters compared to wild-type nuclei (Figure 6D). In a consistent manner, we observed an increased intensity relative heterochromatin fraction in both mutants (Figure 6E).

The spatial distribution of chromocenters is not altered in *kaku1* mutants

We questioned whether changes in nuclear morphology and heterochromatin were accompanied by a spatial re-organization within the nuclear space. We compared observed chromocenter patterns in *kaku1* mutants to an expected organization under a completely random model, conditioned by the shape and size of each nucleus and by the number and size of its chromocenters. The *kaku1-3* nuclei did not show any modification in the spatial organization of chromocenters within the nuclear space, as revealed by the local scale analysis provided by the *F*- and *G*-functions (Figure 7A-B) and the global scale analysis with the *H*-function (Figure 7C). Similarly, analysis with the *B*-function showed that the relative positioning of chromocenters to the nuclear border was not altered (Figure 7D). In *kaku1-4*, the local analysis provided by the *F*-function showed no difference to the random model (Figure 7A), the three other spatial descriptors (related to local, global, and peripheral positioning) showed no differences compared to wild-type nuclei (Figure 7B-D). We thus concluded that KAKU1 does not contribute to the global regular and peripheral positions of chromocenters within the nuclear space.

Discussion

An exhaustive picture of the complex nuclear landscapes in *crwn1*, *crwn2* and *kaku1* mutants

By exploiting a confocal microscopy approach coupled with 3D reconstructions in continuous space and integrating the natural variability structurally present inside a cell nucleus population, we deeply analysed the morphological nuclear parameters in the *crwn1*, *crwn2*, *crwn1 crwn2* and *kaku1* mutants. We confirmed results from previous studies, highlighted differences, quantified new parameters and provided a robust framework, pointing out to the normalisation processes required for result interpretation. For instance, whereas the general tendency on nuclear shape and size in *crwn1* and *crwn1 crwn2* were similar to previous studies, some differences were observed. Sakamoto et al.

(2013) and Wang et al. (2013) reported that the *crwn2* nuclear area in root epidermal cells, 4-week leaves or guard cells was not significantly different from wild-type, whereas Dittmer et al. (2007) and our work highlighted that *crwn2* nuclear area and volume were smaller than the ones of *crwn1* and wild-type nuclei. These discrepancies can have different origins, such as methods (2D versus 3D) or technical cytological approaches (use of different fixative solutions such as ethanol/acetic acid solution or paraformaldhyde). Some discrepancies with previous published data may also come from the biological materials analysed related to cell-type or tissue specificity, and/or growing/environmental conditions. Our data highlight some *crwn1* versus *crwn2* differences, as well as *kaku1-3* versus *kaku1-4*, helping in the characterisation of the mutants, but also opening questions for the underlying mechanisms.

CRWN1 and CRWN2 proteins have a large-scale impact on 3D nuclear organization

We demonstrated that *crwn1* and *crwn2* have an impact on nuclear size and morphology showing smaller and more spherical nuclei and noticed enhanced effects in the double mutant. The data suggest that CRWN1 and CRWN2 share overlapping functions to regulate CC size, nuclear size and shape. The spatial organizations of CCs differed in the three mutations. The *crwn1* mutant displayed a more preferential peripheral organization, with the CCs being as "pulled to the edge". Interestingly, the CC positioning in *crwn2* did not differ from the random model. This is the first time that a random distribution of CCs is reported in Arabidopsis. In the double mutant the CCs tend to cluster preferentially in the inside part of the nucleus. However, due to their smaller nuclei, no alteration on the CCs distances to the border was detected in *crwn1 crwn2*. Hence, CRWN1 and CRWN2 proteins modulate the CC spatial positioning and they may prevent the tendency of the chromocenter to aggregate. From our data we could conclude that CRWN1 and CRWN2 proteins are involved in a large-scale remodelling of nuclei organization. How this is achieved remains to be established. Physical link between CRWN1 and CRWN2 and heterochromatin compartments would be interesting to investigate as well as other parameters. For instance, chromocenter organization could also be constrained by chromosome territories.

Minor changes on nuclear organization driven by KAKU1

The main change in the nuclear morphology in the *kaku1* mutants was an increase in volume exhibited by *kaku1-3,* and a less elongated shape detected for both mutants nuclei, in agreement with previous studies (Tamura et al., 2013; Haraguchi et al., 2016). The data show that the lack of this outer-nuclear membrane protein allows a modulation of nuclei shape. KAKU1 is a nucleo-cytoplasmic linker involved in nuclear movement through the interaction with actin filament and has a putative role on the maintenance of the tension (Tamura et al., 2013; Haraguchi et al., 2016). Therefore, the deformation of nuclei may also result from an altered transfer of the cytoplasmic motor forces or tension on the nuclei. The *kaku1* mutants showed no alteration of the spatial configuration of chromocenters suggesting that size change does not necessary lead to change in spatial distribution of CC and thus, highlighting the specific role of CRWN in this function.

Conclusion

In this paper we applied an implemented toolkit for image and spatial statistical analyses, specifically designed to analyse the 3D nuclear spatial organization with a specific focus on the nuclear morphology and the 3D intra-nuclear distribution of CCs. Here, using the established framework we aim to extract organisational rules and decipher the mechanisms regulating nuclear architecture. We bring new insight on how mutations that affect the plant nuclear envelope impact the nuclear architecture, and thus some genetic determinants of 3D heterochromatin distribution. It seems interesting to further investigate the link between the nuclear periphery and the global nuclear organization by testing other compartments. The developed framework will also allow testing a larger number of nuclear candidates to enlarge the knowledge about nuclear organization. Furthermore, it will be interesting to use it to investigate the 3D nuclear dynamics during developmental processes such as the floral transition, to better understand developmental transcriptional reprogramming at the 3D nuclear level.

Experimental procedure

Plant materials

Arabidopsis thaliana lines used in this study were in the Columbia wild-type background (Col-0). The *crwn1-1* and *crwn2-1* (formerly known as *linc1-1* and *linc2-1*) and *kaku1-3* and *kaku1-4* mutants were described by Dittmer et al. (2007) and Tamura et al. (2013), respectively. Plantlets were grown in vitro at 20 °C, 70 % humidity, 36 µmol m^{-2} s^{-1} and under a 16 hours light / 8 hours dark period. Rosette leaves of nodes 3 to 5 were harvested on plants at the 5.10 developmental growth stage, with an inflorescence of 1 cm high (Boyes et al. 2001). Leaves were immediately fixed in 4% paraformaldehyde in 1 x PBS buffer (PFA), under vacuum 3 times for 1 min each, and three times for 20 min each, on ice. Samples were then incubated overnight in PFA, at 4 °C, washed in 1 x PBS buffer and stored at 4°C until use.

Nucleus staining and imaging

To preserve the 3D nuclear architecture, we analysed nuclei in cryosections following Tirichine et al. (2009), with the following modifications. Leaf samples were incubated in 10% and 20% sucrose for 1 hour each, and 30% sucrose, overnight at 4°C. After removing the excess of sucrose, samples were embedded in Neg-50 Frozen section medium (Thermo scientific), at -30°C. Leaf sections of 20 µm were made on a Cryostar TM NX70 (Thermo scientific), placed on slides coated with poly-L-Lysine (Thermo scientific) and stored at -20°C.

For DAPI (4'6-Diamidino-2-phenylindole) staining, slides were equilibrated at room temperature and washed in 1 x PBS for 5 min to remove embedding medium, then in 100% ethanol for 10 min to remove chlorophyll. After a new wash in 1 x PBS, the sections were covered with 40 µL of 5% acrylamide mix in 1 x PBS and a coverslip. After 1 hour, coverslips were gently removed, and slides were treated with the following successive washes: 10 min in 100% methanol, 2 times 5 min in PBS-Tween 0.05%, 2 times 5 min in PBS, and 30 min in 0.5% PBS-Tween 20 0.5%. After a last wash in 1 x PBS, leaf sections were stained using 5 µg/mL DAPI PBS-0.1% Triton X-100 solution for 10 min.

Samples were then washed in 1 x PBS and mounted in VECTASHIELD antifade mounting medium (Vector laboratories) for confocal imaging. Nuclei images were captured on a ZEISS 710 confocal microscope equipped with a 405 nm diode, using a PL APO X63 oil immersion objective (NA 1.4, WD 190 µm). The 3D stack images with a mean voxel resolution of 0.01 µm in the XY plane and of 0.02 µm in Z-axis were acquired. The anisotropy of voxel sizes in XY-Z was taken into account in the spatial analysis procedures. The final processed 3D stack images were 223 of Col-0 nuclei, 89 of *crwn1*, 59 of *crwn2* and 91 of *crwn1 crwn2*.

Image segmentation

The binary masks of the nuclei and their chromocenters were generated from the DAPI stained 3D confocal image stacks using the methodology previously described (Andrey et al., 2010). Each image was denoised using a 3D median filter and binarized using Otsu's method (Otsu, 1979). The resulting 3D binary mask of the nucleus was enhanced by filling holes and by regularizing shape using opening and closing operations (Soille, 2003). The watershed transform was then applied on the Gaussian gradient of the original DAPI-image to partition the nuclear domain into homogeneous intensity regions.

Mathematical morphological operators were applied a contrast index was computed for each regions, resulting in a specific enhancement of the regions corresponding to chromocenters (Andrey et al., 2010). Automatic thresholding was applied on the contrast index to automatically extract the chromocenters. When needed, the threshold was manually corrected. A triangular surface mesh was computed to represent the 3D envelope of each object (nucleus or chromocenter) by applying the Marching Cubes algorithm (Lorensen and Cline, 1987) on the corresponding binary mask.

Quantitative image analysis

Morphometric measures on nuclei and chromocenters were performed on their 3D binary masks. Object volume was estimated following the Cavalieri's principle, multiplying the number of voxels in the object by the unit voxel

volume. Surface area was estimated using the Crofton's formula (Lang et al., 2001; Lehmann and Legland, 2012) to correct for discretization bias. Sphericity, a normalized shape measure, was computed as: $36\ \pi\ \text{Volume}^2/\text{Area}^3$. This parameter takes a maximum value of 1.0 for a sphere and decreases toward 0.0 as the shape surface becomes less regular. The lengths of the three major axes of each object were computed from the eigenvalues of the inertia matrix of the equivalent ellipsoid. The elongation and flatness shape parameters were calculated. The relative quantity of constitutive heterochromatin was measured using two parameters. The volume heterochromatin fraction, the proportion of nuclear space occupied by chromocenters. The intensity heterochromatin fraction, which is the proportion of total nucleus intensity in chromocenters. Based on the triangular meshes, two measures were used to quantify the positioning of chromocenters relatively to the nuclear border. The distance to the border was defined as the distance between the barycenter of a chromocenter and the nearest point on the nuclear envelope. The spacing to the border was defined as the distance between the closest pair of points between the envelopes of the chromocenter and of the nucleus. Statistical comparison tests between the mutant groups and the control group were performed using the non-parametric Wilcoxon test under the R software (R Development Core Team, 2007).

Statistical analysis of chromocenter spatial configurations

The statistical spatial analysis of chromocenter 3D distributions was performed by comparing observed configurations to expectations under a completely random distribution model. The model was parameterized using observed nuclear size, nuclear shape, number and size of chromocenters. The chromocenters were modelled as equivalent spheres with sizes set to measured volumes on observed nuclei. Simulations generating random patterns of chromocenters within triangular meshes were performed to estimate null distributions under the random model. Chromocenters were prevented from intersecting each other and from intersecting the nuclear surface. Four spatial descriptors were used to quantify the observed and the simulated spatial arrangements of chromocenters. The F-function, the cumulated distribution function of the distance between an arbitrary position in the nucleus and the nearest chromocenter. The G-function, the cumulative distribution function of

the distance between each chromocenter and its nearest neighbour. The H-function, the cumulative distribution function of the distance between each chromocenter and any other one. The B-function, the cumulative distribution function of the distance between each chromocenter and the nuclear envelope. For each nucleus, 99 random patterns were simulated and used to estimate an average under the random model for each of the F-, G-, H- and B-functions. A set of 99 more patterns was generated to estimate the null distribution of the fluctuations of these functions around the average. This was used to compute a Spatial Distribution Index, which is a normalized value between 0 and 1 quantifying the relative position of the observed measures compared to the model (Andrey et al., 2010). One SDI value was obtained for each spatial descriptor. The test of goodness was performed to test the uniformity of the SDI distribution (Andrey et al., 2010).

Acknowledgements

We thank Dr. Paul Fransz for fruitful discussion. We acknowledge and thank Olivier Grandjean and the Cytology and imaging Platform at INRA Versailles. We are grateful to Dr. Eric J. Richards and Dr. Kentaro Tamura for providing seeds of the *crwn* and *kaku1* mutants, respectively. JA and SDP were supported by PhD fellowships, provided by the European Commission Seventh Framework-People-2012-ITN project EpiTRAITS (Epigenetic regulation of economically important plant traits, no-316965). SDP was supported by a short-term fellowship from Swammerdam Institute for Life Sciences, University of Amsterdam. KS was supported by a LabEx Saclay Plant Sciences (ANR-10-LABX-0040-SPS). The funding to support this research provided by the ITN EpiTRAITS, INRA and LabEx SPS is gratefully acknowledged.

References

Aguilar-Arnal, L., Hakim, O., Patel, V.R., Baldi, P., Hager, G.L., and Sassone-Corsi, P. (2013). Cycles in spatial and temporal chromosomal organization driven by the circadian clock. Nat. Struct. Mol. Biol. **20,** 1206-1213.

Andrey, P., Kieu, K., Kress, C., Lehmann, G., Tirichine, L., Liu, Z., Biot, E., Adenot, P.G., Hue-Beauvais, C., Houba-Herin, N., Duranthon, V., Devinoy, E., Beaujean, N., Gaudin, V., Maurin, Y., and Debey, P. (2010). Statistical analysis of 3D images detects regular spatial distributions of centromeres and chromocenters in animal and plant nuclei. PLoS Comput. Biol. **6,** e1000853.

Baroux, C., Pecinka, A., Fuchs, J., Kreth, G., Schubert, I., and Grossniklaus, U. (2016). Non-random chromosome arrangement in triploid endosperm nuclei. Chromosoma.

Boveri, T. (1909). Die Blastomerenkerne von Ascaris megalocephala und die Theorie der Chromosomenindividualität. Arch Zellforsch **3,** 181-268.

Ciska, M., and Moreno, S. (2013). NMCP/LINC proteins: Putative lamin analogs in plants? Plant Signal Behav **8**.

Ciska, M., and Moreno Diaz de la Espina, S. (2014). The intriguing plant nuclear lamina. Front Plant Sci **5,** 166.

Cremer, T., and Cremer, M. (2010). Chromosome territories. Cold Spring Harb. Perspect. Biol. **2,** a003889.

Del Prete, S., Arpon, J., Sakai, K., Andrey, P., and Gaudin, V. (2014). Nuclear architecture and chromatin dynamics in interphase nuclei of Arabidopsis thaliana. Cytogenet. Genome Res. **143,** 28-50.

Dittmer, T.A., Stacey, N.J., Sugimoto-Shirasu, K., and Richards, E.J. (2007). LITTLE NUCLEI genes affecting nuclear morphology in Arabidopsis thaliana. Plant Cell **19,** 2793-2803.

Dixon, J.R., Gorkin, D.U., and Ren, B. (2016). Chromatin Domains: The Unit of Chromosome Organization. Mol. Cell **62,** 668-680.

Fransz, P., De Jong, J.H., Lysak, M., Castiglione, M.R., and Schubert, I. (2002). Interphase chromosomes in Arabidopsis are organized as well defined chromocenters from which euchromatin loops emanate. Proc. Natl. Acad. Sci. U. S. A. **99,** 14584-14589.

Gonzalez-Sandoval, A., and Gasser, S.M. (2016). On TADs and LADs: Spatial Control Over Gene Expression. Trends Genet. **32,** 485-495.

Graumann, K. (2014). Evidence for LINC1-SUN associations at the plant nuclear periphery. PLoS ONE **9,** e93406.

Gruenbaum, Y., and Medalia, O. (2015). Lamins: the structure and protein complexes. Curr. Opin. Cell Biol. **32,** 7-12.

Guelen, L., Pagie, L., Brasset, E., Meuleman, W., Faza, M.B., Talhout, W., Eussen, B.H., de Klein, A., Wessels, L., de Laat, W., and van Steensel, B. (2008). Domain organization of human chromosomes revealed by mapping of nuclear lamina interactions. Nature **453,** 948-951.

Haraguchi, T., Tominaga, M., Nakano, A., Yamamoto, K., and Ito, K. (2016). Myosin XI-I is Mechanically and Enzymatically Unique Among Class-XI Myosins in Arabidopsis. Plant & cell physiology.

Heitz, E. (1929). Heterochromatin, Chromocentren, Chromomeren (Vorlaufige Mitteilung). Ber. Dtsch. Bot. Ges. **47,** 274-284.

Lorensen, W.E., and Cline, H.E. (1987). Marching cubes: a high resolution 3D surface construction algorithm. ACM Computer Graphics **21,** 163–169.

Masuda, K., Xu, Z.J., Takahashi, S., Ito, A., Ono, M., Nomura, K., and Inoue, M. (1997). Peripheral framework of carrot cell nucleus contains a novel protein predicted to exhibit a long alpha-helical domain. Exp. Cell Res. **232,** 173-181.

Meuleman, W., Peric-Hupkes, D., Kind, J., Beaudry, J.B., Pagie, L., Kellis, M., Reinders, M., Wessels, L., and van Steensel, B. (2013). Constitutive nuclear lamina-genome interactions are highly conserved and associated with A/T-rich sequence. Genome Res. **23,** 270-280.

Nemeth, A., Conesa, A., Santoyo-Lopez, J., Medina, I., Montaner, D., Peterfia, B., Solovei, I., Cremer, T., Dopazo, J., and Langst, G. (2010). Initial genomics of the human nucleolus. PLoS Genet. **6,** e1000889.

Otsu, N. (1979). A threshold selection method from gray-level histograms IEEE Transactions on Systems, Man, and Cybernetics **9,** 62-66.

Pawar, V., Poulet, A., Detourne, G., Tatout, C., Vanrobays, E., Evans, D.E., and Graumann, K. (2016). A novel family of plant nuclear envelope-associated proteins. J Exp Bot **67,** 5699-5710.

Pecinka, A., Schubert, V., Meister, A., Kreth, G., Klatte, M., Lysak, M.A., Fuchs, J., and Schubert, I. (2004). Chromosome territory arrangement and homologous pairing in nuclei of *Arabidopsis thaliana* are predominantly random except for NOR-bearing chromosomes. Chromosoma **113,** 258-269.

Pickersgill, H., Kalverda, B., de Wit, E., Talhout, W., Fornerod, M., and van Steensel, B. (2006). Characterization of the Drosophila melanogaster genome at the nuclear lamina. Nat. Genet. **38,** 1005-1014.

Pontvianne, F., Carpentier, M.C., Durut, N., Pavlistova, V., Jaske, K., Schorova, S., Parrinello, H., Rohmer, M., Pikaard, C.S., Fojtova, M., Fajkus, J., and Saez-Vasquez, J. (2016). Identification of Nucleolus-Associated Chromatin Domains Reveals a Role for the Nucleolus in 3D Organization of the A. thaliana Genome. Cell reports **16,** 1574-1587.

Rosa, S., De Lucia, F., Mylne, J.S., Zhu, D., Ohmido, N., Pendle, A., Kato, N., Shaw, P., and Dean, C. (2013). Physical clustering of FLC alleles during Polycomb-mediated epigenetic silencing in vernalization. Genes Dev. **27,** 1845-1850.

Sakamoto, Y., and Takagi, S. (2013). LITTLE NUCLEI 1 and 4 regulate nuclear morphology in Arabidopsis thaliana. Plant Cell Physiol. **54,** 622-633.

Sati, S., and Cavalli, G. (2016). Chromosome conformation capture technologies and their impact in understanding genome function. Chromosoma.

Schubert, V., Berr, A., and Meister, A. (2012). Interphase chromatin organisation in Arabidopsis nuclei: constraints versus randomness. Chromosoma **121,** 369-387.

Soille, P. (2003). Morphological Image Analysis: Principles and Applications. (Springer-Verlag).

Tamura, K., Goto, C., and Hara-Nishimura, I. (2015). Recent advances in understanding plant nuclear envelope proteins involved in nuclear morphology. J Exp Bot **66,** 1641-1647.

Tamura, K., Iwabuchi, K., Fukao, Y., Kondo, M., Okamoto, K., Ueda, H., Nishimura, M., and Hara-Nishimura, I. (2013). Myosin XI-i links the nuclear membrane to the cytoskeleton to control nuclear movement and shape in Arabidopsis. Current biology : CB **23,** 1776-1781.

Tanabe, H., Habermann, F.A., Solovei, I., Cremer, M., and Cremer, T. (2002). Non-random radial arrangements of interphase chromosome territories: evolutionary considerations and functional implications. Mutat. Res. **504,** 37-45.

van Koningsbruggen, S., Gierlinski, M., Schofield, P., Martin, D., Barton, G.J., Ariyurek, Y., den Dunnen, J.T., and Lamond, A.I. (2010). High-resolution whole-genome sequencing reveals that specific chromatin domains from most human chromosomes associate with nucleoli. Mol. Biol. Cell **21,** 3735-3748.

Wang, H., Dittmer, T.A., and Richards, E.J. (2013). Arabidopsis CROWDED NUCLEI (CRWN) proteins are required for nuclear size control and heterochromatin organization. BMC Plant Biol. **13,** 200.

Wijchers, P.J., Geeven, G., Eyres, M., Bergsma, A.J., Janssen, M., Verstegen, M., Zhu, Y., Schell, Y., Vermeulen, C., de Wit, E., and de Laat, W. (2015). Characterization and dynamics of pericentromere-associated domains in mice. Genome Res. **25,** 958-969.

Zhao, H., Sifakis, E.G., Sumida, N., Millan-Arino, L., Scholz, B.A., Svensson, J.P., Chen, X., Ronnegren, A.L., Mallet de Lima, C.D., Varnoosfaderani, F.S., Shi, C., Loseva, O., Yammine, S., Israelsson, M., Rathje, L.S., Nemeti, B., Fredlund, E., Helleday, T., Imreh, M.P., and Gondor, A. (2015). PARP1- and CTCF-Mediated Interactions between Active and Repressed Chromatin at the Lamina Promote Oscillating Transcription. Mol. Cell **59,** 984-997.

Zhao, W., Guan, C., Feng, J., Liang, Y., Zhan, N., Zuo, J., and Ren, B. (2016). The Arabidopsis CROWDED NUCLEI genes regulate seed germination by modulating degradation of ABI5 protein. Journal of integrative plant biology **58,** 669-678.

Zhou, X., Graumann, K., and Meier, I. (2015). The plant nuclear envelope as a multifunctional platform LINCed by SUN and KASH. J Exp Bot **66,** 1649-1659